sustainability

MDPI

Article

Using a Photoacoustic Cell for Spectroscopy of Toxic Air Pollutants including CO_2, SO_2 and NO Gases

Reza Hadjiaghaie Vafaie [1,*] and Ghader Hosseinzadeh [2]

[1] Department of Electrical Engineering, University of Bonab, Bonab 5551761167, Iran
[2] Department of Chemical Engineering, University of Bonab, Bonab 5551761167, Iran
* Correspondence: rzvafaiee@gmail.com or reza.vafaie@ubonab.ac.ir

Abstract: Due to the rise in global temperature and climate change, the detection of CO_2, SO_2 and NO pollutants is important in smart cities. In this paper, an H-shaped photoacoustic cell is utilized for the detection of low-concentration gases. The geometry of the cell is miniaturized and designed with specific parameters in order to increase its efficiency and performance. The designed cell eliminates problems such as bulkiness and cost, which prevent the use of sensors in detecting greenhouse gases. The simplicity of the design expands the application rate of the cell in practice. In order to consider the viscosity and thermal effects, the cell is formulized by fully linearized Navier–Stokes equations, and various parameters, such as acoustic pressure, frequency response, sound speed (sound velocity) and quality factor, are investigated for the mentioned gases. The performance of the system is frequency-based, and the target gases can be detected by using a microelectromechanical resonator as a pressure sensor. Quality factor analysis expresses that CO_2, SO_2 and NO gases have quality factors of 27.84, 33.62 and 33.32, respectively. The performance of the cell in the resonance state can be expressed by the linear correlation between the results. The background noise generated in the photoacoustic research has been removed by miniaturization due to the obtained resonance, and the proposed cell provides a proper signal-to-noise ratio. The results of the proposed system represent the increase in the quality factor, which reduces the losses and thus increases the sensitivity of the system in the study of greenhouse gases.

Keywords: greenhouse gases (GHGs); photoacoustic spectroscopy; gas sensing; microsystem

Citation: Hadjiaghaie Vafaie, R.; Hosseinzadeh, G. Using a Photoacoustic Cell for Spectroscopy of Toxic Air Pollutants including CO_2, SO_2 and NO Gases. *Sustainability* **2023**, *15*, 9225. https://doi.org/10.3390/su15129225

Academic Editors: Ali Elkamel and Ali Ahmadian

Received: 22 February 2023
Revised: 6 June 2023
Accepted: 6 June 2023
Published: 7 June 2023

1. Introduction

In recent decades, air pollution has caused significant hazards to both human health and the environment [1]. Indeed, the problem of air pollution has reached a threshold of considerable danger. Air pollution has been considered as a major threat to the planet, and human activities such as transportation have global-scale effects upon the environment, the ozone layer and human health [1,2]. Nowadays, greenhouse gas emissions are higher than ever and have had a major impact on global climate change [2]. Unprecedented global warming has been attributed to human activities due to increased greenhouse gas emissions [2]. The combustion of fossil fuels at the final stage of usage releases significant amounts of greenhouse gases [3,4]. Their combustion products are the main cause of global problems such as greenhouse effects, ozone depletion, acid rain and environmental pollution; therefore, their use has a harmful impact [3,4]. Greenhouse gas emissions and global warming not only affect the environment and the economy, but also have significant effects on human health [3,5]. Hazardous gas leakage leads to very dangerous situations if not detected quickly. Human environmental safety is a top priority, and an efficient gas detection system is required. NO_X and carbon monoxide are two main pollutants emitted by the transportation system, and they cause serious environmental pollution; air pollutants including CO_2, SO_2 and NO have an effective role in respiratory problems (including bronchitis, emphysema and asthma) [6]. Toxic gases containing CO_2, SO_2 and NO, even

in lower concentrations, have many impacts on human health. The reliable detection of various gases in low concentrations is necessary in sectors such as industrial production, environmental monitoring, air quality assurance, automotive technology, etc. [7]. The main source of SO_2 emissions is the combustion of fossil fuels. The typical concentration of SO_2 in industrial exhaust is at the ppm level (particle per molecule). However, SO_2 has considerable impacts on environmental pollution (e.g., acid rain) [8].

Nitric oxide (NO) is one of the most common air pollutants found in nitrogen oxides (NO_x) in various ratios (x). Nitrogen oxides are important components which, in addition to helping form acid rain and the greenhouse effect, have a great impact on human health, such as in diseases of the respiratory system and, consequently, other vital diseases. The significant effects of NO include the deterioration of lung function due to the prolonged exposure to this gas and the increased risk of respiratory disease [9]. NO_2 gas detection has already been studied in [4,5]. The increment of carbon dioxide emissions (which is another effect of gasoline combustion) is related to global warming. The rapidly rising atmospheric concentration of carbon dioxide (CO_2) has been considered as a major factor in climate change [10]. The air pollution arising from energy consumption is an important threat to the environment; therefore, the hazardous effects of air pollution on health have attracted much attention in recent years [11]. Thus, the accurate measurement of toxic gases is of considerable importance, not only in industry but also in everyday human life in smart cities.

Practical applications such as industrial control processes and long term environmental monitoring require sensitive and selective concentration measurements over long time periods by automatic monitoring devices. In recent decades, PA spectroscopy has been regarded as a highly sensitive and selective measurement and detection method under delicate laboratory conditions. Photoacoustic instruments can be employed for online, long-term and totally automatic industrial-process monitoring. Photoacoustic spectroscopy is an effective and inexpensive method which utilizes sound and light for the purpose of studying the properties of materials in solid, gas and liquid states. In this paper, a photoacoustic cell consisting of two miniaturized buffers and a resonator are used in order to detect and investigate CO_2, SO_2 and NO gases. In the last ten years, photoacoustic devices have played an important role in applications such as industrial production [12], medicine and spectroscopy [13]. In [14], Thomas Strah et al. investigated a promising idea known as intrinsic miniaturization, i.e., using a typical MEMS microphone as a miniaturized PA cell for photoacoustic trace gas sensing. The obtained results showed that using the MEMS microphone directly as a PA cell offered the possibility of an extremely miniaturized, highly sensitive and very cost-efficient photoacoustic trace gas sensor. In [15], Vafaie et al. used photoacoustic cells in order to investigate pollutants produced by the automotive industry, and the results showed a high potential for photoacoustic cells to expand sensitive laser sensors. An infrared photoacoustic system is considered as a common method for long-term gas measurement [5,15].

Most of the proposed techniques suffer from cross-sensitivity to water. One of the important issues for most gas detectors is selectivity in the presence of water vapor. Therefore, the detection of a target gas in humid air is different than in dry conditions. In [5], Vafaie and et al. designed a miniaturized photoacoustic cell for hydrogen gas detection; the effects of various parameters, such as frequency response, quality factor, acoustic pressure and the temperature effect on the device, were analyzed by the finite element method (FEM). Based on the results, the frequency analysis in the hydrogen gas medium indicates that the first natural frequency of the sensor was 88.563 kHz, a 65 kHz difference to the second natural frequency. The photoacoustic-based measurement technique is based on generating an acoustic wave in the gas, which is accomplished by the absorption of a modulated laser beam (Figure 1a). As shown in Figure 1b, when the gas molecules absorb the laser beam, they are excited to higher energy levels. When these molecules return to the base level, their excess energy is released as heat. Pressure changes are generated by thermal expansion and appear in the form of an acoustic wave. This acoustic wave is detected

by using a conventional pressure sensor, such as an MEMS-based resonator [16]. Broadly speaking, the photoacoustic cell-based gas detection consists of four steps, including [5]: (1) amplitude and frequency modulating of the laser radiation at a wavelength at which the target species shows high absorption; (2) stimulation of the target molecules by absorption of the incident radiation; (3) non-radiative transfer of the absorbed energy via collisions with other molecules, hence resulting in periodic joule heating at the modulation frequency; (4) detection of the acoustic waves produced by the heating with the pressure sensors.

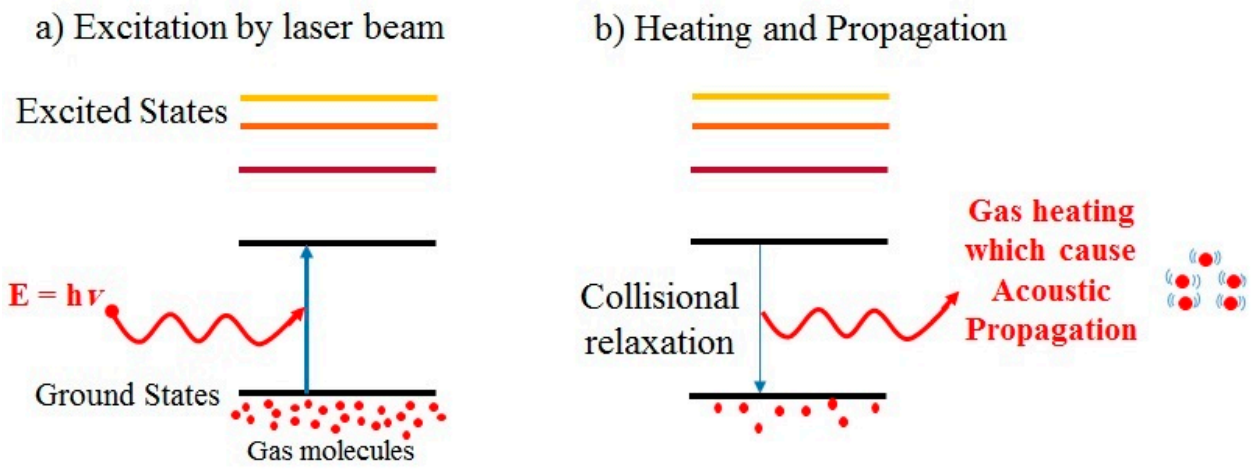

Figure 1. Photoacoustic phenomenon from excitation to propagation.

As described in [17], in the case of vibrational excitation, radiative emissions do not play a crucial role because the radiative lifetimes of the vibrational levels are longer than the time required to deactivate the collision at pressures commonly used in photoacoustics.

The goal of the current research is to enhance the performance of the sensor in order to detect CO_2, SO_2 and NO gases. An air pollutant sensor must meet a set of basic requirements, including:

1. High selectivity for detection of target gas rather than different gases, and high sensitivity for detecting low concentrations of substances;
2. Large dynamic domain for monitoring gas components at different concentrations using a unique tool.

Photoacoustic spectroscopy satisfies these requirements, which enables this technique to represent significant advantages in the detection of pollutant gases [18]. In addition, photoacoustic sensors can be used to detect gases in hazardous environments or in the presence of high-temperature or strong electromagnetic interference [19]. Using the photoacoustic effect to measure the concentration of gases is an appealing option in the field of optical detection methods. Although this method has been widely used to measure gases in recent decades, its potential as an ultra-sensitive and small device has not been thoroughly investigated yet [20]. Until now, much research has been conducted in the field of gas detection in various sectors, including:

Yong Hugh Liu et al., 2019, examined the reduction process of air pollutants and greenhouse gases in the transportation sector [21]. In 2018, Kalathur S. V. Santhanam et al. conducted studies on the effects of greenhouse gases on the atmosphere and the importance of detecting them [22]. Trieu-Vuong Dinh et al., 2016, conducted research on improving the performance of infrared sensors for use in various sectors, which showed the improvement and development of the performance of these sensors, especially in monitoring air pollution, for which they are in great demand today [16]. J. Rouxela et al., 2015, proposed a photoacoustic sensor which uses an acoustic method to increase the signal level and also improve the detection of minimum concentrations of gas. In order

to simplify the sensor for use in various applications and to reduce costs, they used a miniature photoacoustic cell with photoacoustic spectroscopy for detecting gases [23].

A.V. Gorelik et al., 2010, utilized a miniature photoacoustic cell to detect carbon dioxide, which showed a decrease in background noise and an increase in cell function [24].

Based on these studies, a conclusion can be drawn that miniaturization has a considerable effect on frequency response, noise and quality factor. In addition, due to the importance of detecting toxic gases containing CO_2, SO_2 and NO at low concentrations, we considered the H-shaped photoacoustic cell to be the optimal structure. The goal was to use this structure in the interest of improving its performance for the detection of target gases. In this study, the theory and physics behind photoacoustic sensing will be described in Section 2. It should be noted that the finite element method (FEM) is the most flexible numerical method for modeling a photoacoustic cell. The ability to handle any type of cell geometry is the advantage of using the FEM model. The properties of the photoacoustic cell were investigated in order to detect CO_2, SO_2 and NO pollutants, and parameters such as resonance frequency, quality factor and sound velocity were calculated for the target gases. In Section 3, a set of simulations will be described which were performed to investigate the effects of frequency response, natural frequencies, acoustic pressure and the heat field inside the proposed cell. Finally, this work is concluded in the Section 4.

2. Theory

The mathematical model for the photoacoustic effect has been in development since the mid-1970s, beginning with a theoretical description of the photoacoustic effect on solids [25]. In reference [25], Duggen et al. investigate the frequency response of photoacoustic cells for gas detection by transferring contaminated gases to a two-volume buffer cell and a resonator. The measurement of other resonance frequencies, as well as parameter modification and the geometrical dimensions of the photoacoustic cell, are important. We investigated the resonance behavior of an H-shaped cylindrical cell by using a mathematical model in the photoacoustic cell which specifically included the effects of pressure. The common model employed in acoustics relies on solving the Helmholtz equations for pressure, which are based on solid presumptions related to the absence of a dissipation mechanism [26]. Approximate models have been established in order to consider heat and viscous losses in boundary layers. In this paper, Navier–Stokes linearized equations are employed for mathematical modeling of the sound wave propagation in the presence of viscous and thermal boundary layers [27]. Here, the harmonic changes are assumed to be neglectable. In order to complete the partial differential equations (PDE), the continuity, motion and energy conservation equations are employed here:

$$i\omega\left(\frac{\widetilde{P}}{P_0}+\frac{\widetilde{T}}{T_0}\right)+\nabla.\widetilde{u}=0 \tag{1}$$

$$i\omega\rho_0\widetilde{u}=-\nabla\widetilde{p}+\nabla.(\mu(\nabla\widetilde{u}+\nabla\widetilde{u}^T)\ +\ \left(\eta-\frac{2\mu}{3}\right)(\nabla.\widetilde{u})I) \tag{2}$$

$$i\omega\rho_0C_p\widetilde{T}=-\nabla.\left(\kappa\nabla\widetilde{T}\right)+i\omega\widetilde{p}+Q_e \tag{3}$$

where $\widetilde{p}$, $\widetilde{T}$ and $\widetilde{u}$ are the pressure, temperature and velocity fields in gases, respectively. P_0, T_0 and ρ_0 are the mean values of the pressure, temperature and density fields, respectively. η and μ are volumetric and shear viscosities. κ, C_p and Q_e are thermal conductivity, heat capacity at constant pressure and volumetric heat source, respectively. I is the characteristic matrix [28]. The heat source is expressed as Equation (4), and the Gaussian profile for the laser beam is assumed.

$$Q_e=aI_0\exp\left[-2\left(\frac{r^2}{\omega^2}\right)\right] \tag{4}$$

where r is the radial coordinate, ω is the radius of laser beam, a is the absorption coefficient and I_0 is the power of the laser beam [29]. In acoustics, several hypotheses make it possible to simplify the aforementioned Navier–Stokes equations. The changes are assumed to involve very low pressure, temperature and gas compression velocity. Equation (5) expresses this hypothesis. Variables with zero subtitles indicate the mean values of quantities, and variables with tildes indicate small changes in the average values of the quantities [30].

$$\begin{cases} P = P_0 + \widetilde{P} \\ T = T_0 + \widetilde{T} \\ U = U_0 + \widetilde{U} \\ \rho = \rho_0 + \widetilde{P} \end{cases} \quad (5)$$

2.1. Cell Design

Photoacoustic cells are a type of optical sensor which are utilized to detect several gases. The photoacoustic spectroscopy technique is in accordance with the absorption of photons by gas molecules and the creation of sound waves [28]. The main features of this photoacoustic cell for gas detection are small size, simplicity, low gas consumption and fast response. Table 1 presents the input parameters of the designed cell:

Table 1. Geometrical dimensions of the cell.

Parameter	Description	Value [cm]
L_{res}	Length of the resonator	0.6
L_{buf}	Length of the buffer	0.3
R_{res}	Radius of the resonator	0.3
R_{buf}	Radius of the buffer	$3 \times R_{res}$

The miniaturization has the following advantages:

(1) These sensors are highly sensitive, but the bulkiness and cost of the sensors prevent them from being used in applications such as greenhouse gas monitoring or indoor air monitoring. Therefore, there is a tendency to miniaturize them [28].
(2) Given that the photovoltaic signal is reversely related to the volume of the chamber, one solution to improve the accuracy of the sensor is to reduce its dimensions [31].
(3) The most common noise in photoacoustic systems, which is due to the absorption of light in cell windows, is reduced by miniaturizing the resonator diameter [18]. In this study, a H-type micro-photoacoustic cell was utilized in order to investigate CO_2, SO_2 and NO gases, as shown in Figure 2. The H-type resonant cell is very simple in its design, with two buffers. The design of the buffer cylinders, as well as the dimensions of the cylinders, are important for the creation of an efficient photoacoustic cell.

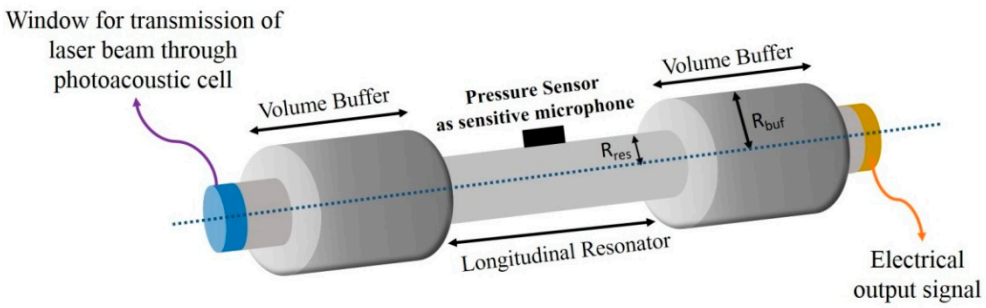

Figure 2. Modeled photoacoustic cell.

2.2. Boundary Conditions

In a resonator, when the length of the buffer volume is 1/4 of the length of the cylinder ($L_{res} = 2L_{buf}$), the maximum known noise interference occurs in the buffers and the operation of the buffers increases as the sound filters. Therefore, the external factors cannot influence the produced acoustic signal inside the cell [32]. The frequency of acoustic resonance modes generated in cylindrical cells is calculated by Equation (6):

$$F_{mnq} = \frac{c}{2}\left(\left(\frac{\alpha_{mn}}{R}\right)^2 + \left(\frac{q}{L}\right)^2\right)^{\frac{1}{2}} \quad (6)$$

where c is the sound velocity and α_{mn} is the nth zero of the derivative of the mth Bessel function at $r = R$. The parameters R and L are the radius and length of the cylinder, respectively. The normal modes are separated into longitudinal (q), radial (n) and azimuthal (m) modes [33]. The cell walls are considered rigid, and non-slip boundary conditions are applied to the gas. In addition, since the thermal conductivity of metal is much greater than that of gas, it is presumed that the walls are isothermal, heading towards zero thermal perturbation in the walls [34]. In general, the no-slip boundary conditions are applied to the velocity field and adiabatic conditions to the temperature in the system. These two conditions are known as the standard boundary conditions for sound pressure. Standard acoustic pressure boundary conditions are applied in order to prevent any thermal or adhesive boundary layers in the walls (layers are negligible). Eigenmode has a quality factor (Q) that describes the energy stored in the resonator relative to the energy lost in a full period, which is expressed as Equation (7):

$$Q = \frac{f_{res}}{BW} \quad (7)$$

where f_{res} is the resonant frequency and BW is the bandwidth. The lower bandwidth results in a higher quality factor and lower surface losses [35]. When the photoacoustic signal is not excited at the resonant frequency, it has a low and very unstable amplitude, and in the non-resonant mode, sound is not propagated and standing waves are not formed, so the effect of photoacoustic resonance is very crucial [34]. In [34], Ishaku et al. optimized the structure of photoacoustic cell buffers, and the results showed that a short diameter with a short buffer length produced high resonance frequency in the photoacoustic cell. A significant component of optimizing both signal amplitude and signal to noise (SNR) ratio is the geometric design of the cell [36]. During photoacoustic measurement, a measured sample is commonly located in an acoustically isolated cell for the sake of increasing the signal and reducing the noise [37]. The cell is frequently used as a sound resonator, and its features considerably affect the measurement results [38].

2.3. Simulation

The COMSOL Multiphysics FEM (finite element method) software was employed to simulate a miniaturized photoacoustic cell to investigate CO_2, SO_2 and NO gases. It should be noted that our simulation study was verified by [3]. The parameters in Table 1 were selected in such a way that the system is able to increase the target signal and, at the same time, minimize both the negative role of the window background signal and external noise for the selected mode. The effect of various parameters was investigated in this study by simulating the miniaturized H-shape geometry. The simulation study of the photoacoustic cell for target gas detection in the FEM model was validated using the experimental results from [28]. It should be noted that the cell was filled by the gases at 293 °C and a pressure of 1 atmosphere.

3. Results and Discussion

In this section, in order to analyze the greenhouse gases, as mentioned before, a photoacoustic cell was used. It was simulated by employing the finite element method

and applying boundary conditions. The influence of different parameters was investigated when the simulated cell was filled with the CO_2, SO_2 and NO gases.

3.1. Acoustic Pressure

Figure 3 represents the acoustic pressure for carbon dioxide gas. The goal was to find the best position for the pressure gauge sensor, where the pressure would reach its maximum. Based on the results obtained from Figure 3, it can be concluded that the maximum pressure for carbon dioxide occurred at the first natural frequency, 18.101 kHz, which indicates the appropriate location for the sensitive microphone (i.e., pressure sensor). The same FEM analysis was performed for different gases, and it was also observed that the maximum pressure for different gases occurred at the first natural frequency; for the CO_2, SO_2 and NO gases, these were 18.101, 26.888 and 23.329 kHz, respectively. Hence, the first natural frequency is considered as the resonance frequency for the target gas.

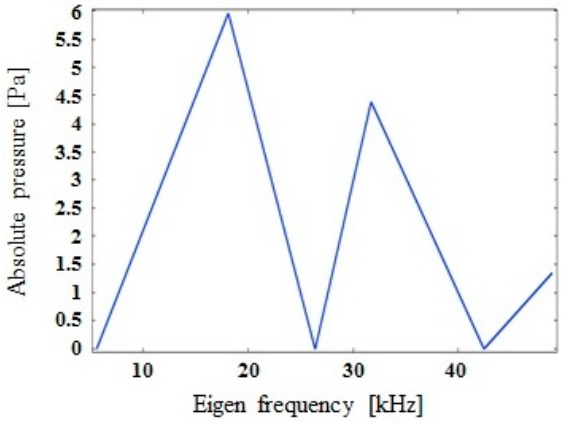

Figure 3. Eigen frequency versus pressure of photoacoustic cell (the cell filled by carbon dioxide molecules).

3.2. Frequency Response

The frequency response of the proposed system is shown in Figure 4. The main point in designing a sensor is to select the proper resonance frequency for a target gas as an excitation frequency of the photoacoustic cell. Thus, studying the frequency response is of great importance.

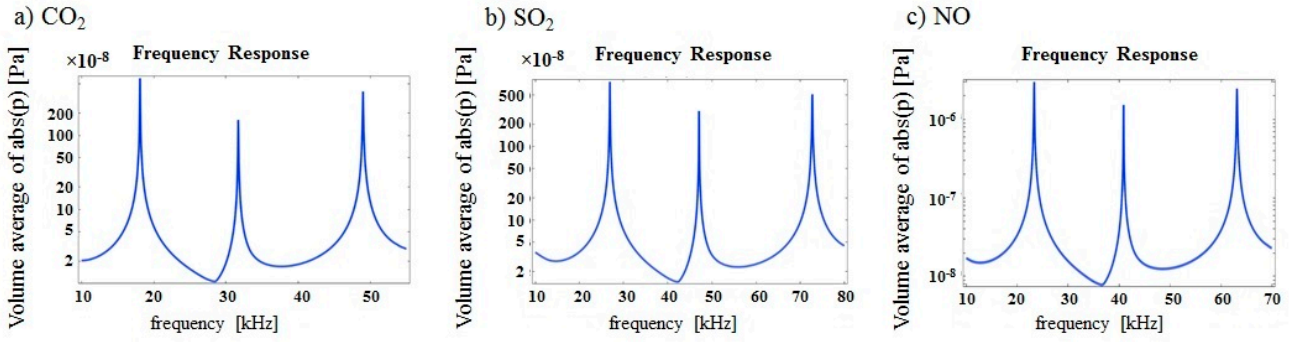

Figure 4. Frequency response of the cell; (**a**) carbon dioxide, (**b**) sulfur dioxide, (**c**) nitric oxide.

At low resonant frequencies, higher noise levels are observed, which results in a further reduction in the signal-to-noise ratio. According to Figure 4, it can be seen that miniaturization solved the problem of low resonance frequencies, because the smaller the diameter of the resonator, the better the signal-to-noise ratio. Based on the results acquired in the acoustic pressure section, the main resonant frequencies for carbon dioxide CO_2, sulfur dioxide SO_2 and nitric oxide NO were 18.101, 26.888 and 23.329 kHz, respectively. The quality factor can be calculated using the frequency response curve. Both the

frequency response and quality factor were calculated in order to evaluate the proposed cell's performance.

3.3. Quality Factor

According to Equation (7), the quality factors of carbon dioxide, sulfur dioxide and nitric oxide gases were calculated, and the results are shown in Table 2.

Table 2. Quality factors and frequency results.

Gas	1st Natural Frequency	2nd Natural Frequency	3rd Natural Frequency	Quality Factor
CO_2	18.101 (kHz)	31.718 (kHz)	48.997 (kHz)	27.84
SO_2	26.888 (kHz)	47.114 (kHz)	72.782 (kHz)	33.32
NO	23.329 (kHz)	40.891 (kHz)	63.158 (kHz)	33.61

The results shown in Table 2 express that another advantage of miniaturization is achieving a high quality factor. A low quality factor indicates high losses, which reduce the cell's sensitivity. Resonance frequency and quality factor are related to losses. It should be pointed out that the results of reference [39] represent that longitudinal resonance modes with high quality factors generate the highest photoacoustic signals.

3.4. Temperature

The photoacoustic effect is produced using a mechanical wave that travels on the surface of the material and is then detected using a pressure sensor. Therefore, for the purpose of calculating acoustic behaviors, the sound velocity must be calculated. Several factors affect the resonant frequency, and these factors depend on the sound velocity. The sound velocity changes with temperature, and a change in temperature results in a change in the resonance frequency. Figure 5 shows the changes in sound velocity versus the changes in temperature.

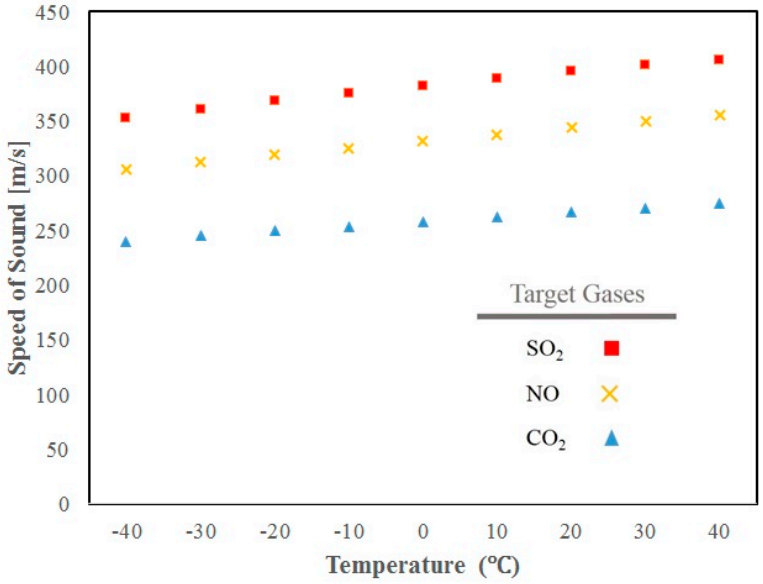

Figure 5. Speed of sound changes for different temperatures.

Temperature is one of the major influential environmental factors in the practical applications of photoacoustic spectroscopy. Temperature changes must be considered to be remarkable for the purpose of avoiding a non-resonant state and obtaining enhanced performance in photoacoustic spectroscopy. Therefore, the measurements of the frequency

response at different temperatures were examined. Figure 6 shows that an increase in temperature led to an increase in the frequency response in the cell, which indicates the function of the cell in the resonance state. The results show that the frequency response increases or decreases directly according to the temperature.

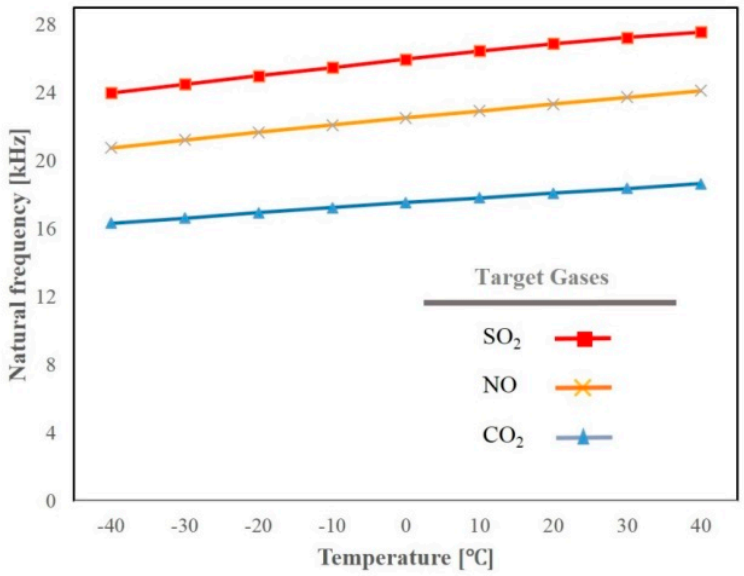

Figure 6. Frequency response changes for different temperatures.

4. Conclusions

In this study, the design and description of miniaturized photoacoustic cells were investigated for the detection of CO_2, NO and SO_2 gases. The finite element method was used in the interest of investigating the frequency response, quality factor, temperature and sound velocity. The results of the obtained frequencies show that the most suitable place for the pressure sensor is where the first natural frequency occurs, which is considered as the resonance frequency. This frequency is 18.101, 23.329 and 26.888 kHz for the CO_2, NO and SO_2 gases, respectively. We studied an optimal photoacoustic cell to investigate the aforementioned gases. Due to the fact that affecting factors of the frequency response depend on sound velocity, the results were investigated inside the cell based on changes in sound velocity at different temperatures, as well as changes in frequency response versus changes in sound velocity. The linear correlation between the obtained results (increase in temperature results in an increase in the sound velocity; increase in sound velocity increases the frequency response) indicates the performance of the cell in the resonance state. The obtained resonance expresses that the background noise generated in the photoacoustic studies was removed by miniaturization, and that the proposed cell has a proper signal-to-noise ratio. These results show that the proposed model provides accurate measurements of the resonant frequency, sound velocity and quality factor. Photoacoustic spectroscopy reveals that it has high sensitivity and accuracy for detecting greenhouse gases. The results of this research are useful and will be efficient for environmental science and smart city studies. For future research, it is suggested that the device be fabricated and that the effect of background noise be evaluated.

Author Contributions: Conceptualization and writing, R.H.V.; review & editing, G.H. All authors have read and agreed to the published version of the manuscript.

Funding: This research received no external funding.

Informed Consent Statement: Not applicable.

Data Availability Statement: Data is unavailable due to privacy.

Conflicts of Interest: The authors declare no conflict of interest.

Nomenclature

Parameter	Description
$\widetilde{p}$	Pressure field
$\widetilde{T}$	Temperature field
$\widetilde{u}$	Velocity field
P_0	Mean value of the pressure
T_0	Mean value of the temperature
ρ_0	Mean value of the temperature
K	Thermal conductivity
C_p	Heat capacity at constant pressure
Q_e	Volumetric heat source
r	Radial coordinate
ω	Radius of laser beam
a	Absorption coefficient
I	Characteristic matrix
I_0	Power of the laser beam
c	Sound velocity
R	Radius of the cylinder
L	Length of the cylinder
f_{res}	Resonant frequency
BW	Bandwidth

References

1. Zhang, M.; Shi, L.; Ma, X.; Zhao, Y.; Gao, L. Study on Comprehensive Assessment of Environmental Impact of Air Pollution. *Sustainability* **2021**, *13*, 476. [CrossRef]
2. Fulton, L.; Lah, O.; Cuenot, F. Transport Pathways for Light Duty Vehicles: Towards a 2° Scenario. *Sustainability* **2013**, *5*, 1863–1874. [CrossRef]
3. Zhang, C.; Wang, Q.; Yin, X. Photoacoustic spectroscopy for detection of trace C_2H_2 using ellipsoidal photoacoustic cell. *Opt. Commun.* **2021**, *487*, 126764. [CrossRef]
4. Li, S.; Lu, J.; Shang, Z.; Zeng, X.; Yuan, Y.; Wu, H.; Pan, Y.; Sampaolo, A.; Patimisco, P.; Spagnolo, V.; et al. Compact quartz-enhanced photoacoustic sensor for ppb-level ambient NO_2 detection by use of a high-power laser diode and a grooved tuning fork. *Photoacoustics* **2022**, *25*, 100325. [CrossRef] [PubMed]
5. Vafaie, R.H.; Pour, R.S.; Nojavan, S.; Jermsittiparsert, K. Designing a miniaturized photoacoustic sensor for detecting hydrogen gas. *Int. J. Hydrogen Energy* **2020**, *45*, 21148–21156. [CrossRef]
6. Shi, L.; Zhang, M.; Zhang, Y.; Yang, B.; Sun, H.; Xu, T. Comprehensive Analysis of Nitrogen Deposition in Urban Ecosystem: A Case Study of Xiamen City, China. *Sustainability* **2018**, *10*, 4673. [CrossRef]
7. Cuesta-Mosquera, A.P.; Wahl, M.; Acosta-López, J.G.; García-Reynoso, J.A.; Aristizábal-Zuluaga, B.H. Mixing layer height and slope wind oscillation: Factors that control ambient air SO_2 in a tropical mountain city. *Sustain. Cities Soc.* **2019**, *52*, 101852. [CrossRef]
8. Mulmi, S.; Thangadurai, V. Semiconducting SnO_2-TiO_2 (S-T) composites for detection of SO_2 gas. *Ionics* **2016**, *22*, 1927–1935. [CrossRef]
9. Pasupuleti, K.S.; Ghosh, S.; Jayababu, N.; Kang, C.-J.; Cho, H.D.; Kim, S.-G.; Kim, M.-D. Boron doped g-C_3N_4 quantum dots based highly sensitive surface acoustic wave NO2 sensor with faster gas kinetics under UV light illumination. *Sens. Actuators B Chem.* **2023**, *378*, 133140. [CrossRef]
10. Sohrabi, S.; Khreis, H.; Lord, D. Impacts of Autonomous Vehicles on Public Health: A Conceptual Model and Policy Recommendations. *Sustain. Cities Soc.* **2020**, *63*, 102457. [CrossRef]
11. Fugiel, A.; Burchart-Korol, D.; Czaplicka-Kolarz, K.; Smoliński, A. Environmental impact and damage categories caused by air pollution emissions from mining and quarrying sectors of European countries. *J. Clean. Prod.* **2017**, *143*, 159–168. [CrossRef]
12. Sadiek, I.; Mikkonen, T.; Vainio, M.; Toivonen, J.; Foltynowicz, A. Optical frequency comb photoacoustic spectroscopy. *Phys. Chem. Chem. Phys.* **2018**, *20*, 27849–27855. [CrossRef] [PubMed]
13. Devabharathi, N.; Umarji, A.M.; Dasgupta, S. Fully Inkjet-Printed Mesoporous SnO_2-Based Ultrasensitive Gas Sensors for Trace Amount NO_2 Detection. *ACS Appl. Mater. Interfaces* **2020**, *12*, 57207–57217. [CrossRef] [PubMed]
14. Strahl, T.; Steinebrunner, J.; Weber, C.; Wöllenstein, J.; Schmitt, K. Photoacoustic methane de-tection inside a MEMS microphone. *Photoacoustics* **2023**, *29*, 100428. [CrossRef]

15. Vafaie, R.H.; Pour, R.S.; Mohammadzadeh, A.; Asad, J.H.; Mosavi, A. Photoacoustic Detection of Pollutants Emitted by Transportation System for Use in Automotive Industry. *Photonics* **2022**, *9*, 526. [CrossRef]
16. Dinh, T.-V.; Choi, I.-Y.; Son, Y.-S.; Kim, J.-C. A review on non-dispersive infrared gas sensors: Improvement of sensor detection limit and interference correction. *Sens. Actuators B Chem.* **2016**, *231*, 529–538. [CrossRef]
17. Tavakoli, M.; Tavakoli, A.; Taheri, M.; Saghafifar, H. Design, simulation and structural optimization of a longitudinal acoustic resonator for trace gas detection using laser photoacoustic spectroscopy (LPAS). *Opt. Laser Technol.* **2010**, *42*, 828–838. [CrossRef]
18. Sthel, M.; Marcelo, G.; Guilherme, L.; Mila, V.; Juliana, R.; Delson, S.; Castro, M.P.; Miklos, A.; Vargas, H. Detection of Greenhouse Gases Using the Photoacoustic Spectroscopy. In *Greenhouse Gases-Emission, Measurement and Management*; IntechOpen: London, UK, 2012.
19. Bonilla-Manrique, O.E.; Posada-Roman, J.E.; Garcia-Souto, J.A.; Ruiz-Llata, M. Sub-ppm-Level Ammonia Detection Using Photoacoustic Spectroscopy with an Optical Microphone Based on a Phase Interferometer. *Sensors* **2019**, *19*, 2890. [CrossRef]
20. Palzer, S. Photoacoustic-Based Gas Sensing: A Review. *Sensors* **2020**, *20*, 2745. [CrossRef]
21. Liu, Y.H.; Liao, W.Y.; Li, L.; Huang, Y.T.; Xu, W.J.; Zeng, X.L. Reduction measures for air pollu-tants and greenhouse gas in the transportation sector: A cost-benefit analysis. *J. Clean. Prod.* **2019**, *207*, 1023–1032. [CrossRef]
22. Santhanam, K.S.V.; Ahamed, N.N.N. Greenhouse Gas Sensors Fabricated with New Materials for Climatic Usage: A Review. *Chemengineering* **2018**, *2*, 38. [CrossRef]
23. Rouxel, J.; Coutard, J.-G.; Gidon, S.; Lartigue, O.; Nicoletti, S.; Parvitte, B.; Vallon, R.; Zéninari, V.; Glière, A. Development of a Miniaturized Differential Photoacoustic Gas Sensor. *Procedia Eng.* **2015**, *120*, 396–399. [CrossRef]
24. Gorelik, A.V.; Ulasevich, A.L.; Nikonovich, F.N.; Zakharich, M.P.; Firago, V.A.; Kazak, N.S.; Starovoitov, V.S. Minia-turized resonant photoacoustic cell of inclined geometry for trace-gas detection. *Appl. Phys. B* **2010**, *100*, 283–289. [CrossRef]
25. Duggen, L.; Albu, M.; Willatzen, M.; Rubahn, H.-G. Modeling Frequency Response of Photoacoustic Cells using FEM for Determination of N-heptane Contamination in Air: Experimental Validation. Available online: https://portal.findresearcher.sdu.dk/en/publications/modeling-frequency-response-of-photoacoustic-cells-using-fem-for- (accessed on 21 February 2023).
26. Ni, F.; Miguel-Brebion, M.; Nicoud, F.; Poinsot, T. Accounting for acoustic damping in a helm-holtz solver. *AIAA J.* **2017**, *55*, 1205–1220. [CrossRef]
27. Berggren, M.; Bernland, A.; Noreland, D. Acoustic boundary layers as boundary conditions. *J. Comput. Phys.* **2018**, *371*, 633–650. [CrossRef]
28. Rouxel, J.; Coutard, J.-G.; Gidon, S.; Lartigue, O.; Nicoletti, S.; Parvitte, B.; Vallon, R.; Zéninari, V.; Glière, A. Miniaturized differential Helmholtz resonators for photoacoustic trace gas detection. *Sens. Actuators B Chem.* **2016**, *236*, 1104–1110. [CrossRef]
29. Sathiyamoorthy, K.; Kolios, M.C. Experimental design and numerical investigation of a photoacoustic sensor for a low-power, continuous-wave, laser-based frequency-domain photoacoustic microscopy. *J. Biomed. Opt.* **2019**, *24*, 121912. [CrossRef]
30. Strumendo, M. Solution of the incompressible Navier-Stokes equations by the method of lines. *Int. J. Numer. Methods Fluids* **2015**, *80*, 317–339. [CrossRef]
31. Glière, A.; Barritault, P.; Berthelot, A.; Constancias, C.; Coutard, J.-G.; Desloges, B.; Duraffourg, L.; Fedeli, J.-M.; Garcia, M.; Lartigue, O.; et al. Downsizing and Silicon Integration of Photoacoustic Gas Cells. *Int. J. Thermophys.* **2020**, *41*, 16. [CrossRef]
32. Cai, Y.; Arsad, N.; Li, M.; Wang, Y. Buffer structure optimization of the photoacoustic cell for trace gas de-tection. *Optoelectron. Lett.* **2013**, *9*, 233–237. [CrossRef]
33. Yehya, F.; Chaudhary, A.K.; Srinivas, D.; Muralidharan, K. Study of thermal decomposition mechanisms and low-level detection of explosives using pulsed photoacoustic technique. *Appl. Phys. B Laser Opt.* **2015**, *121*, 193–202. [CrossRef]
34. Ishaku, L.; Hutson, D. A Resonant Photoacoustic CO_2 Sensor Based on MID-IR LED and MEMS Microphone Technology Operating at 4.3 µM. *Innov. Syst. Des. Eng.* **2016**, *7*, 1–11.
35. Baumann, B.; Wolff, M.; Kost, B.; Groninga, H.G. Calculation of Quality Factors and Amplitudes of Photo-Acoustic Resonators. Available online: https://www.researchgate.net/publication/271075875_Calculation_of_Quality_Factors_and_Amplitudes_of_Photoacoustic_Resonators (accessed on 21 February 2023).
36. Duggen, L.; Frese, R.; Willatzen, M. FEM analysis of cylindrical resonant photoacoustic cells. *J. Phys. Conf. Ser.* **2010**, *214*, 012036. [CrossRef]
37. Gorelik, A.V.; Ulasevich, A.L.; Nikonovich, F.N.; Zakharich, M.P.; Chebotar, A.I.; Firago, V.A.; Stetsik, V.M.; Kazak, N.S.; Starovoitov, V.S. Small-Size Resonant Photoacoustic Cell of Inclined Geometry for Gas Detection. *arXiv* **2009**, arXiv:0910.1005.
38. Suchenek, M. A Novel Method of Evaluating the Frequency Response of a Photoacoustic Cell. *Int. J. Thermophys.* **2014**, *35*, 2287–2291. [CrossRef]
39. Yehya, F.; Chaudhary, A.K. Designing and modeling of efficient resonant photo acoustic sensors for spectro-scopic applications. *J. Mod. Phys.* **2011**, *2*, 200. [CrossRef]